


# High-power terahertz quantum cascade lasers with $\sim 0.23$ W in continuous wave mode

Cite as: AIP Advances 6, 075210 (2016); <https://doi.org/10.1063/1.4959195>

Submitted: 04 May 2016 • Accepted: 08 July 2016 • Published Online: 26 July 2016

Xuemin Wang, Changle Shen,  Tao Jiang, et al.

## COLLECTIONS

 This paper was selected as Featured



View Online



Export Citation



CrossMark

## ARTICLES YOU MAY BE INTERESTED IN

[Thermoelectrically cooled THz quantum cascade laser operating up to 210 K](#)

Applied Physics Letters **115**, 010601 (2019); <https://doi.org/10.1063/1.5110305>

[High power terahertz quantum cascade lasers with symmetric wafer bonded active regions](#)

Applied Physics Letters **103**, 171113 (2013); <https://doi.org/10.1063/1.4826943>

[Terahertz quantum cascade VECSEL with watt-level output power](#)

Applied Physics Letters **113**, 011104 (2018); <https://doi.org/10.1063/1.5033910>

Celebrate **Open Access Week** With



LEARN MORE

## High-power terahertz quantum cascade lasers with ~0.23 W in continuous wave mode

Xuemin Wang,<sup>1</sup> Changle Shen,<sup>1</sup> Tao Jiang,<sup>1</sup> Zhiqiang Zhan,<sup>1</sup>  
 Qinghua Deng,<sup>1</sup> Weihua Li,<sup>1</sup> Weidong Wu,<sup>1,a</sup> Ning Yang,<sup>2</sup> Weidong Chu,<sup>2</sup>  
 and Suqing Duan<sup>2</sup>

<sup>1</sup>Research Center of Laser Fusion, China Academy of Engineering Physics, Mianyang,  
 621900, Sichuan, P. R. China

<sup>2</sup>Institute of Applied Physics and Computational Mathematics, Beijing, 100088, P. R. China

(Received 4 May 2016; accepted 8 July 2016; published online 26 July 2016)

Terahertz quantum cascade lasers with a record output power up to ~0.23 W in continuous wave mode were obtained. We show that the optimal 2.9-mm-long device operating at 3.11 THz has a low threshold current density of 270 A/cm<sup>2</sup> at ~15 K. The maximum operating temperature arrived at ~65 K in continuous wave mode and the internal quantum efficiencies decreased from 0.53 to 0.19 for the devices with different cavity lengths. By using one convex lens with the effective focal length of 13 mm, the beam profile was collimated to be a quasi Gaussian distribution. © 2016 Author(s). All article content, except where otherwise noted, is licensed under a Creative Commons Attribution (CC BY) license (<http://creativecommons.org/licenses/by/4.0/>). [<http://dx.doi.org/10.1063/1.4959195>]

Due to its unique qualities such as low energy, the ability to penetrate into many opaque materials, the especial excitations for many materials at terahertz (THz) range, and so on, THz wave shows many potential important applications.<sup>1,2</sup> In these fields, low-cost, compact, coherent high-power sources are especially needed. Among all THz sources, terahertz quantum cascade lasers (THz QCLs) are the most suitability to meet the above requirements. Since the first demonstration in 2002,<sup>3</sup> THz QCLs have witnessed a rapid development. Till date, the frequency ranges from 1.2 to 5.0 THz<sup>4,5</sup> and the highest output power in pulsed wave (PW) mode achieves more than 1 W.<sup>6,7</sup> However, the output power in continuous wave (CW) mode is still limited to 138 mW since 2006.<sup>8</sup> This is an impediment toward many important applications in spectroscopy, imaging, remote sensing, *etc.*<sup>9,10</sup> Therefore, improving the CW output power is one of the most important research goals in the fields.

Amanti M.I. and Lianhe Li, *et al.*<sup>11,12</sup> once proposed an active region with a hybrid bound-to-continuum transition and resonant phonon extraction. Using this structure, the PW output power can be greatly increased and achieves more than 1 W from a single facet.<sup>12</sup> However, no obvious improvement of the CW output power ( $P_{CW}$ ) has been acquired. It is known that the high threshold current density and electrical power consumption of the laser increase the self-heating and results in the degradation of the gain,<sup>13</sup> which is especially evident for the lasers working in CW mode. Therefore, reducing the threshold current density and the electrical power consumption by optimizing material growth and device process is necessary as that for mid-infrared QCLs.<sup>14</sup>

The design we use here is a hybrid bound-to-continuum transition and resonant phonon extraction similar to that of Amanti M.I. and Lianhe Li, *et al.*<sup>11,12</sup> The layer sequence of one period for the active region is as following: **5.2/10.3/1.7/10.75/3.6/8.8/3.95/17.2** nm (The numbers in normal are the thickness of the GaAs wells, in bold are that of Al<sub>0.15</sub>Ga<sub>0.85</sub>As barriers, and the underscored layer is doped with Si to  $3.0 \times 10^{16}$  cm<sup>-3</sup>). The growth sequence comprised a 700-nm-thick GaAs buffer layer doped to  $2.5 \times 10^{18}$  cm<sup>-3</sup>, followed by 200 repeats of an active region, and finally a 50-nm-thick GaAs contact layer with heavily Si-doped to  $5.0 \times 10^{18}$  cm<sup>-3</sup>. Then, the wafer was

<sup>a</sup>Author to whom correspondence should be addressed. Electronic mail: [wuweidongding@163.com](mailto:wuweidongding@163.com)

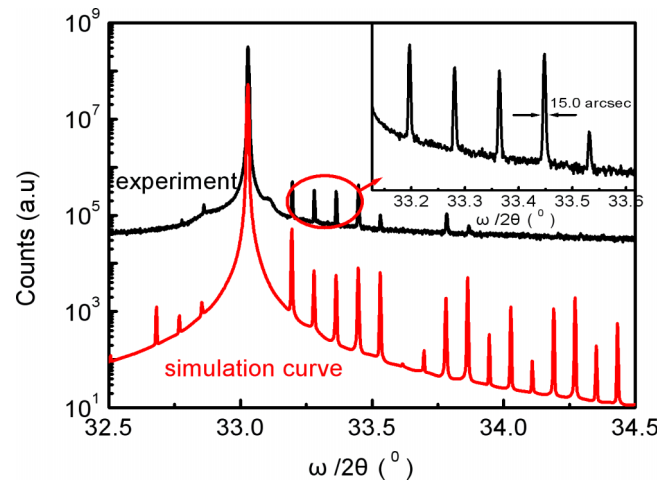


FIG. 1. High resolution XRD spectrum from the wafer and the theoretical simulation curve for the structure. The inset shows the expanded view of the first satellite peaks.

processed by optical lithography and wet chemical etching to form the ridges. An Ge/Au/Ni/Au (26/54/15/150 nm) layer was evaporated on top of the ridge and two 25- $\mu\text{m}$ -wide narrow metal bars were formed on each side of the ridged region. For wire bonding, a Ti/Au (5/200 nm) layer were deposited on both the top of the ridge and the bottom contact layer. The substrate was thinned down to  $\sim 200\ \mu\text{m}$  and a Ti/Au layer was deposited on the back of the device for die mounting. An  $\text{Al}_2\text{O}_3/\text{Ti}/\text{Au}/\text{Ti}/\text{Al}_2\text{O}_3$  (200/10/100/10/200 nm) high-reflectivity coating was evaporated on the rear facet. Ridges with different cavity lengths (from 1.5 mm to 4.5 mm) and the same width (175  $\mu\text{m}$ ) were fabricated. Finally, the devices were indium soldered on the copper heat-sinks and wire-bonded.

Fig. 1 shows the HRXRD spectrum from the wafer and a theoretical simulation curve for the design structure. The HRXRD curve indicates clear satellite peaks, associated with 200 superlattice repeat periods, that corresponds closely to the simulation curve. An active region thickness of 61.71 nm was obtained from the spacing of the satellite peaks, which was in excellent agreement with the design thickness of 61.5 nm (+0.34% error). This demonstrates the high degree precision of the active region growth. The inset presents an expanded view of the first satellite peaks. The averaged full-width at half-maximum (FWHM) for the first four satellite peaks is about 15.0 arcsec. This value is very small and can be due to the good layer homogeneity and little interface roughness.<sup>15,16</sup>

Fig. 2 depicts the experimental setup used to measure the  $P_{\text{CW}}$ . THz QCLs were mounted on the cold finger of a liquid-helium continuous-flow cryostat equipped with a 3.0-mm-thick polyethylene (PE) window. The measured transmission of the window in the THz range was  $\sim 71.7\%$ . An f/2.0 OC-NI Winston cone (Entrance=1.98 mm, Exit=8.22 mm, Length=20.47 mm) was put

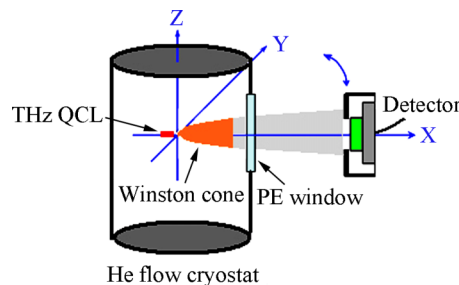


FIG. 2. Schematic diagram of the experimental setup for measuring the CW output power of the THz QCLs. The distance between the laser front facet and the detector is 4 cm.

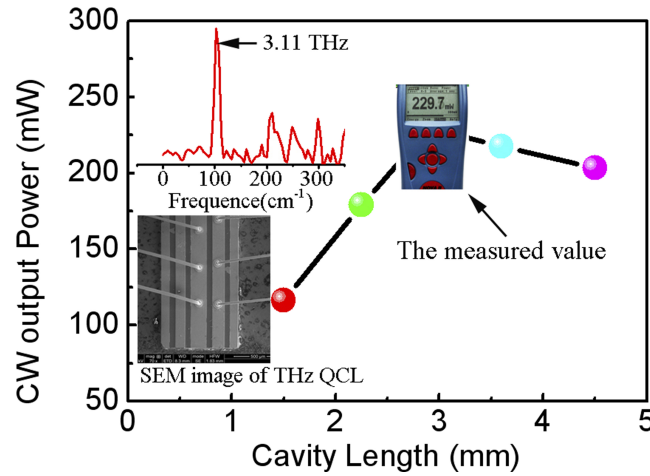


FIG. 3. The CW output power vs. the cavity length at  $\sim 15$  K. The above inset is the typical lasing spectrum at  $\sim 15$  K. The down inset is the SEM image of the device.

in front of the laser facet to increase the collection efficiency. The light intensity was measured by a room temperature detector (OPHIR 3A-P-THz). Due to the limitation of the detector aperture (diameter=12 mm), the light was not entirely collected. Like previous Ref. 17, by the integration of intensity and spatial distribution, the collection efficiency was rudely estimated to be  $\sim 80.6\%$ . However, none of the CW powers presented in this paper were corrected by the transmission of the PE window and the collection efficiency.

Fig. 3 presents the dependencies of  $P_{CW}$  on the cavity lengths ( $L$ ) of THz QCLs at a heat sink temperature of  $\sim 15$  K. A maximum  $P_{CW}$  up to  $\sim 0.23$  W was obtained from the device with a 2.9-mm-long cavity and a 175- $\mu\text{m}$ -wide ridge. The achieved maximum  $P_{CW}$  outperforms the previous reported  $P_{CW}$ . Further, it seems that there exists an obvious change for the scaling factor  $dP_{CW}/dL$ . For the devices with  $L \leq 2.9$  mm, the  $P_{CW}$  is nearly linear with  $L$  as observed in some previous reports<sup>7,12</sup> and  $dP_{CW}/dL$  is  $\sim 83$  mW/mm. When  $L$  is longer than 2.9 mm,  $dP_{CW}/dL$  is  $\sim 28$  mW/mm. This suggests an optimal  $L$  ( $\sim 2.9$  mm) for the  $P_{CW}$  of the THz QCLs. The inset displays the typical lasing spectrum of the device at a heat sink temperature of  $\sim 15$  K centered at 3.11 THz, 0.29 THz lower than that of the designed 3.40 THz. As described previously,<sup>18</sup> the performance of THz QCLs was limited by the interplay of the optical phonon scattering of thermal electrons and parasitic current. There exists an optimal frequency around 3.0 THz for the least degradation of the laser gain with the temperature. Therefore, our reduced frequency to 3.11 THz may improve the performance of the devices and thus the  $P_{CW}$ .

The output power-current-voltage (PIV) characteristics of the devices with different  $L$  were exhibited in Fig. 4. All devices worked at about 15 K. Threshold current densities ( $J_{th}$ ) of  $\sim 230$  mA/cm<sup>2</sup> to  $\sim 304$  mA/cm<sup>2</sup> were obtained for the devices with increasing  $L$ . Following Ref. 19, the waveguide loss can be expressed as  $\alpha_w = J_{th}g\Gamma - \alpha_m$ , where  $J_{th}$ ,  $g$ ,  $\Gamma$  and  $\alpha_m$  are the threshold current density, the gain coefficient, the mode overlap factor with active region and the effective mirror loss ( $\alpha_m = \frac{1}{2L} \ln(\frac{1}{R_1R_2})$ ), where  $R_1$  and  $R_2$  are the reflectivity coefficient of the front facet and the rear facet, respectively. To the high-reflectivity coating,  $R_2$  can be achieved as  $\sim 1$  by calculating the one-dimensional Helmholtz equation (the real parts of the refractive index of the Al<sub>2</sub>O<sub>3</sub> and Au are 1.20 and 11.88, respectively and the effective refractive index of the active region is 3.3) and  $R_1=0.32$ .<sup>20</sup> Thus, we can extract  $\alpha_m \approx 3.80$  cm<sup>-1</sup> to  $1.27$  cm<sup>-1</sup> for the different devices. Further, by comparing the acquired  $J_{th}$  between the devices with different  $L$ ,  $\alpha_w \approx 15.4$  cm<sup>-1</sup> to  $5.6$  cm<sup>-1</sup> were obtained for the different devices. Such waveguide loss values are in agreement with the reported value  $7.0$  cm<sup>-1</sup>,<sup>21</sup> which can be due to the little carrier absorption. The inset presents the  $P_{CW}$  with different heat sink temperature for  $L=1.5$  mm and  $2.25$  mm. The maximum operating temperature is about 65 K for  $L=2.25$  mm. The slope efficiencies of  $\sim 269$  mW/A,  $\sim 218$  mW/A,  $\sim 120$  mW/A,  $\sim 91$  mW/A and  $\sim 89$  mW/A were achieved from the devices with increasing  $L$ . The relation between

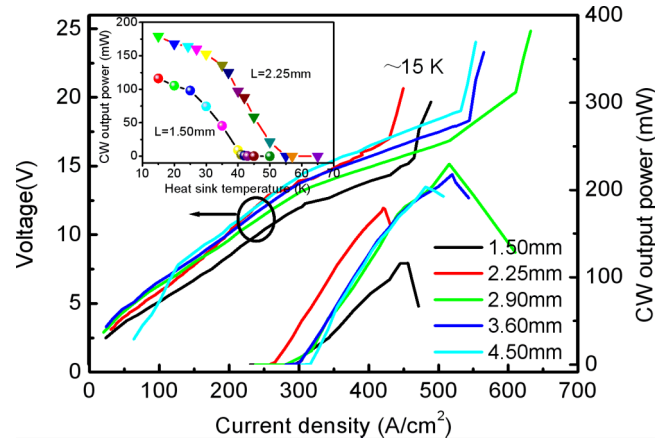


FIG. 4. Measured voltage/CW output power vs. current density with different cavity lengths at  $\sim 15$  K. The inset depicts the CW output power vs. heat sink temperature for 1.5 mm-long and 2.25 mm-long devices (The voltage incremental step of the measurement is about 0.5 V).

the slope efficiency ( $dP/dI$ ) and the internal quantum efficiency of one period ( $\eta_i$ ) has been obtained by Williams *et al.*<sup>22</sup> Thus,  $\eta_i$  can be given as

$$\eta_i = \frac{e}{h\nu N_p} \left(1 + \frac{\alpha_w}{\alpha_m}\right) \frac{dP}{dI} \quad (1)$$

where  $e$  is the elemental electronic charge,  $h\nu$  is the photon energy,  $N_p$  is the repeat periods of the active region. Using the obtained slope efficiencies, the above  $\alpha_m$  and  $\alpha_w$ , the internal quantum efficiencies were calculated as 0.53, 0.50, 0.30, 0.21 and 0.19, respectively. It seems that one injected electron generates 106, 99, 60, 43 and 37 photons through all periods in the active region for the devices with increasing  $L$ , respectively. Finally, the wall-plug efficiencies ( $E_w$ ) from 0.64% to 0.29% can be obtained, which indicates that  $E_w$  reduces as  $L$  increases.

According to the antenna model for wire lasers,<sup>23</sup> the far-field amplitude is mainly determined by the longitudinal factor

$$F_i^Z = \frac{\sin(\varphi_+)}{\varphi_+} \mp \frac{\sin(\varphi_-)}{\varphi_-} \quad (2)$$

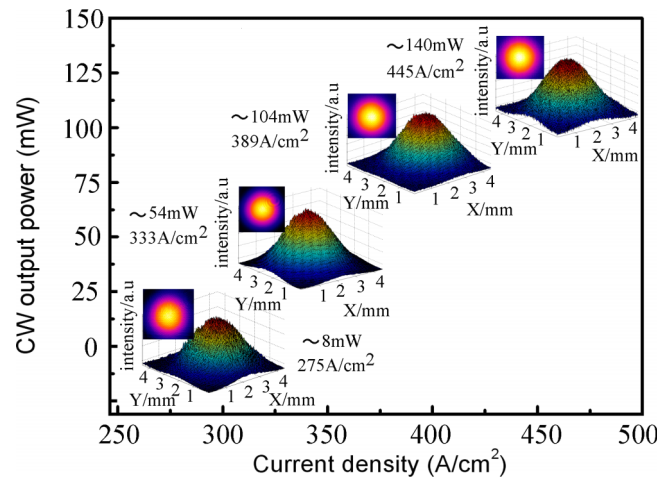


FIG. 5. Three-dimensional (3D) intensity distribution of the QCL beam vs. current density using an external convex lens. The measurement is obtained by an uncooled micro-bolometer array with  $320 \times 240$  pixels on a pitch of  $23.5 \mu\text{m}$ . To protect the detector, 1 to 3 numbers of papers were placed in front of the detector.

where  $\varphi_{\pm} = \pi [c/c_L \pm \cos(\psi)]L/\lambda$  are the phase differences for the radiation,  $\psi$  is an angle between the longitudinal axis and the direction to the observation point,  $c$  is the velocity of light and  $c_L$  is the longitudinal phase velocity. From Eq. (2), the beam profile of THz QCLs is known to be axially symmetric with maximum amplitudes in some directions. In our case,  $c_L/c \approx 3.3$ ,<sup>23</sup>  $\lambda = 96.5 \mu\text{m}$  (3.11 THz) and  $L = 1.5 \text{ mm}$  to  $4.5 \text{ mm}$ , the divergence angles were calculated about  $20.6^\circ$  to  $11.9^\circ$ . To reduce the divergence angle, we employed an external convex lens with an effective focal length of 13 mm. The results show that the divergence angle can be decreased to below  $3^\circ$ . Fig. 5 presents the three-dimensional (3D) intensity distribution of the beam using one convex lens. Obviously, by the collimation of one convex lens, the ringlike beam patterns due to the interference of the radiation emitted from different parts, end and side facets of the laser bar<sup>18</sup> seem to be effectively depressed. The intensity distribution appears uniform and forms a quasi Gaussian distribution regardless of the current density.

In conclusion, we have demonstrated high power THz QCLs up to  $\sim 0.23 \text{ W}$  in continuous wave mode at  $\sim 15 \text{ K}$ . The low threshold current density (Minimum:  $230 \text{ mA/cm}^2$ ) and high wall-plug efficiency (Maximum:  $0.64\%$ ) have been achieved. Moreover, by using one convex lens, the beam profiles have been effectively improved to be a quasi Gaussian distribution. This dramatic increase in output power in continuous wave mode and optimization of the beam profiles leads to a new opportunity for THz spectroscopy and sensing.

The authors acknowledge the help from Lianhe Li, University of Leeds, Leeds. The project was financially supported by Ministry of National Science and Technology Special Major Instrument Program (No. 2011YQ130018) and National Key Scientific Instrument and Equipment Development Project of China (No. 2014YQ090709).

- <sup>1</sup> A. D. Rakić, T. Taimre, K. Bertling, Y. L. Lim, P. Dean, D. Indjin, Z. Ikonić, P. Harrison, A. Valavanis, S. P. Khanna, M. Lachab, S. J. Wilson, E. H. Linfield, and A. G. Davies, *Opt. Express* **21**, 22194 (2013).
- <sup>2</sup> J. P. Guillet, B. Recur, L. Frederique, B. Bousquet, L. Canioni, I. Manek-Honninger, P. Desbarats, and P. Mounaix, *J. Infrared Milli Terahertz Waves* **35**, 382 (2014).
- <sup>3</sup> R. Kohler, A. Tredicucci, F. Beltram, H. E. Beere, E. H. Linfield, A. G. Davies, D. A. Ritchie, R. C. Iotti, and F. Rossi, *Nature* **417**, 156 (2002).
- <sup>4</sup> C. Walther, M. Fischer, G. Scalari, R. Terazzi, N. Hoyler, and J. Faist, *Appl. Phys. Lett.* **91**, 131122 (2007).
- <sup>5</sup> C. W. I. Chan, Q. Hu, and J. L. Reno, *Appl. Phys. Lett.* **101**, 151108 (2012).
- <sup>6</sup> M. Brandstetter, C. Deutsch, M. Krall, H. Detz, D. C. Macfarland, T. Zederbauer, A. M. Andrews, W. Schrenk, G. Strasser, and K. Unterrainer, *Appl. Phys. Lett.* **103**, 171113 (2013).
- <sup>7</sup> L. H. Li, J. X. Zhu, L. Chen, A. G. Davies, and E. H. Linfield, *Opt. Express* **23**, 2720 (2015).
- <sup>8</sup> B. S. Williams, S. Kumar, Q. Hu, and J. L. Reno, *Electron. Lett.* **42**, 89 (2006).
- <sup>9</sup> M. Locatelli, M. Ravaro, S. Bartalini, L. Consolino, M. S. Vitiello, R. Cicchi, F. Pavone, and P. D. Natale, *Sci. Rep.* **5**, 13566 (2015).
- <sup>10</sup> M. Amanti, G. Scalari, M. Beck, and J. Faist, *Opt. Express* **20**, 2772 (2012).
- <sup>11</sup> M. I. Amanti, G. Scalari, R. Terazzi, M. Fischer, M. Beck, J. Faist, A. Rudra, P. Gallo, and E. Kapon, *New J. Phys.* **11**, 125022 (2009).
- <sup>12</sup> L. Lianhe, C. Li, Z. Jiangxuan, J. Freeman, P. Dean, A. Valavanis, A. G. Davies, and E. H. Linfield, *Electron. Lett.* **50**, 309 (2014).
- <sup>13</sup> H. K. Lee and J. S. Yu, *Solid-State Electron.* **54**, 769 (2010).
- <sup>14</sup> M. S. Vitiello, G. Scalari, B. Williams, and P. D. Natale, *Opt. Express* **23**(4), 5167 (2015).
- <sup>15</sup> H. E. Beere, J. R. Freeman, O. P. Marshall, C. H. Worrall, and D. A. Ritchie, *J. Cryst. Growth* **311**, 1923 (2009).
- <sup>16</sup> H. E. Beere, J. C. Fowler, J. Alton, E. H. Linfield, D. A. Ritchie, R. Kohler, A. Tredicucci, G. Scalari, L. Ajili, J. Faist, and S. Barbieri, *J. Cryst. Growth* **278**, 756 (2005).
- <sup>17</sup> A. J. L. Adam, I. Kašalynas, J. N. Hovenier, T. O. Klaassen, J. R. Gao, E. E. Orlova, B. S. Williams, S. Kumar, Q. Hu, and J. R. Reno, *Appl. Phys. Lett.* **88**, 151105 (2006).
- <sup>18</sup> Y. Chassagneux, Q. J. Wang, S. P. Khanna, E. Strupiechonski, J. R. Coudeville, E. H. Linfield, A. G. Davies, F. Capasso, M. A. Belkin, and R. Colombelli, *IEEE Transaction on Terahertz Science and Technology* **2**(1), 83 (2012).
- <sup>19</sup> C. Gmachl, F. Capasso, D. L. Sivco, and A. Y. Cho, *Rep. Prog. Phys.* **64**, 1533 (2001).
- <sup>20</sup> S. Kohen, B. S. Williams, and Q. Hu, *J. Appl. Phys.* **97**, 053106 (2005).
- <sup>21</sup> L. Junqi, C. Jianyan, W. Tao, L. Yanfang, L. Fengqi, L. Lu, W. Lijun, and W. Zhanguo, *Solid-State Electron.* **81**, 68 (2013).
- <sup>22</sup> B. S. Williams, H. Callebaut, S. Kumar, Q. Hu, and J. L. Reno, *Appl. Phys. Lett.* **82**, 1015 (2003).
- <sup>23</sup> E. E. Orlova, J. N. Hovenier, T. O. Klaassen, I. Kašalynas, A. J. L. Adam, J. R. Gao, T. M. Klapwijk, B. S. Williams, S. Kumar, and Q. Hu, *Phys. Rev. Lett.* **96**, 173904 (2006).